Open Access

Fabrication of Black Silicon With Thermostable Infrared Absorption by Femtosecond Laser

Chun-Hao Li
Ji-Hong Zhao
Xin-Yue Yu
Qi-Dai Chen
Jing Feng
Hong-Bo Sun, *Member, IEEE*
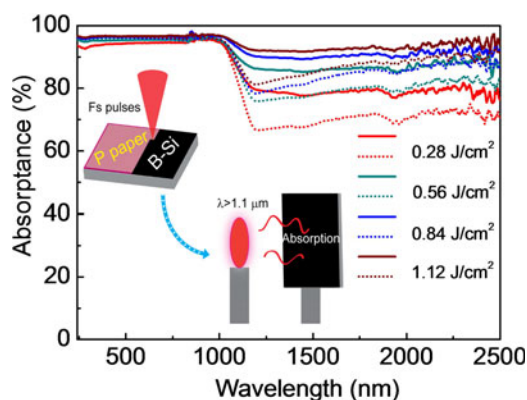
Fabrication of Black Silicon With Thermostable Infrared Absorption by Femtosecond Laser

Chun-Hao Li, Ji-Hong Zhao, Xin-Yue Yu, Qi-Dai Chen, Jing Feng, and Hong-Bo Sun, *Member, IEEE*

State Key Laboratory on Integrated Optoelectronics, College of Electronic Science and Engineering, Jilin University, Changchun 130023, China

Abstract: Annealing-insensitive black silicon with high absorption below the silicon bandgap has been achieved by femtosecond laser direct writing. Spike microstructures with sizes ranging from 4 to 25 μm are formed on the surface layer of silicon substrate, and a large amount of phosphorous impurities (10^{21} cm^{-3}) is doped during the resolidification process. The infrared absorption of phosphorus-doped black silicon decreases slightly with both the annealing temperature and duration. Excitingly, the largest decrease is less than 10% at 2 μm (annealing 240 min at 873K). This thermostable infrared absorption is related to free carrier absorption. After laser irradiation, the phosphorus-doped layer maintains a relatively high crystallinity that can be improved further during thermal annealing. The density of the electrically activated impurities is approximately 10^{19} cm^{-3}.

Index Terms: Femtosecond laser, phosphorous doping, black silicon, infrared absorption.

1. Introduction

Femtosecond (fs) laser irradiation is one of the most attractive fabrication approaches of black silicon (B-Si) [1]–[4]. The sulfur-doped (S-doped) B-Si in sulfur hexafluoride (SF$_6$) atmosphere has a near-uniform absorption from ultraviolet to near-infrared [1]–[3]. Therefore, it is very attractive for use in the manufacture of optoelectronic devices, such as infrared photovoltaics [5], [6]. However, the below-band-gap radiation absorption of S-doped B-Si is unstable with respect to annealing (an essential step in the preparation of semiconductor devices) due to the non-thermal equilibrium doping of S. It is well known that S atoms have an extremely small impurity-separation coefficient ($\sim 10^{-5}$) and a very low solid solubility (3×10^{16} cm^{-3}) in the Si substrate [7], [8]. As a result, thermal annealing can dramatically reduce the S concentration in the top layer of B-Si and can then reduce the infrared absorption. Although annealing-insensitive B-Si with high infrared absorption was obtained by Peng *et al.*, the stable infrared absorption of their sample is induced by the free carrier absorption of the highly doped (10^{18} cm^{-3}, 0.01–0.02 $\Omega \cdot$ cm) substrate [9]. Using this substrate, it is difficult to construct a semiconductor device-based p-n junction or a Schottky junction. Therefore, to obtain a B-Si that can both retain high infrared absorption after annealing and form a semiconductor junction, phosphorus (P) is introduced as a dopant into the surface layer of Si via fs laser irradiation.

Compared to S, P shows the following advantages in the Si substrate. First, P has a much larger separation coefficient (0.36) and higher solid solubility (1.3×10^{21} cm^{-3}) than does S [10]. This means that the absorption of P-doped Si would be stable during thermal annealing due to a slow impurity diffusion process [9]. Second, the lattice distortion of the Si substrate induced by P dopants is much smaller because the atomic radius of P is close to that of Si. In the present work, highly P-doped B-Si is fabricated by fs laser irradiation, with the doping concentration in the top layer reaching up to 5×10^{20} cm^{-3}. Experiments have shown that the below-band-gap absorption of P-doped B-Si is insensitive to thermal annealing. Based on this excellent performance, it is possible to apply the modified B-Si to the fabrication of optoelectronic devices such as infrared photodectectors and solar cells [11]–[14].

2. Experiments

Si(111) wafers (n-type, 250 μm thick, 1500 Ω·cm) are cut into 10×10 mm^2 or 15×15 mm^2 samples for subsequent experimental analyses. These Si substrates are cleaned using a standard cleaning solution [28]. Solid-state diffusion N70X (referred as "phosphorus paper" in the following discussion) is used as the source of P dopants. Prior to the fs laser irradiation, phosphorus paper is tailored and is placed on the Si substrate. A few drops of alcohol are dropped to eliminate the air gap between the phosphorus paper and Si substrate. Then, the Si-Phosphorus paper complex is placed into a vacuum cavity filled with 0.1 MPa argon as the protective gas. The sample is then irradiated by a Ti:Sapphire fs laser amplifier (Spectra-Physics, 800 nm center wavelength, 100 fs pulse duration, and 1 kHz repetition rate). Laser spot is focused down to 260 μm in diameter by a 600 mm focal length lens. To obtain large-area patterns of Si surface (10×10 mm^2 for Hall-effect analyses and 15×15 mm^2 for absorption measurement), the vacuum cavity is mounted on a 2-D translation stage controlled by a computer program. Si wafers covered with the phosphorus paper are translated in the S-line sweep at a rate of 1 mm/s, and the spacing between two adjusted lines is 65 μm such that each spot is exposed to 816 laser pluses.

The optical properties of the samples are measured using a Shimadzu UV-3600 spectrophotometer equipped with an integrating sphere (LISR-UV3100). With the spectrophotometer, the total hemispherical (specular and diffuse) reflectance (R) and transmittance (T) of samples are measured in the range of 0.25~2.5 μm in 2 nm increments, and the absorptance ($A = 1 - R - T$) is calculated at each wavelength. The surface morphology images are obtained using a field emission scanning electron microscope (SEM, JSM-7500F, JEOL, and Japan). Raman spectra are obtained using a LabRAM HR Evolution Raman Spectrometer by HORIBA Scientific with a 532 nm laser. The doping concentrations of P in the Si substrate before and after the annealing are analyzed by second ion mass spectrometry (SIMS). This instrument is equipped with a CAMECA 6F device using a 10 keV Cs$^+$ primary beam at an incident angle of 25 degrees from the surface normal. The electrical properties are measured using an ACCENT HL5500PC Hall system and all measurements were performed at room temperature.

3. Result and Discussions

Fig. 1(a)–(d) show the surface morphologies (titled 45°) of P-doped B-Si samples (SPL1~SPL4) fabricated at four different laser fluences of 0.28, 0.56, 0.84, and 1.12 J/cm^2, respectively. Spike structures are observed after the laser irradiation in the entire scanning ablation region. With increasing laser fluence, the height of surface structures increases while their density decreases. The actual height (observed height in the SEM images $\times\sqrt{2}$) of spikes for SPL1~SPL4 are 4~8 μm (Fig. 1(a), SPL1), 9~13 μm (Fig. 1(b), SPL2), 14~16 μm (Fig. 1(c), SPL3), and 19~25 μm (Fig. 1(d), SPL4).

The absorptances of SPL1~SPL4 are shown in Fig. 1(e). Compared to the crystalline Si substrate (the green line), all of the P-doped B-Si samples show a higher absorptance at the wavelength region from 0.25 to 2.5 μm before annealing. As the laser fluence increases, the absorptance below the band gap (or infrared light region, $\lambda = 1.1 \sim 2.5\,\mu$m) increases from ~78% to ~95%.
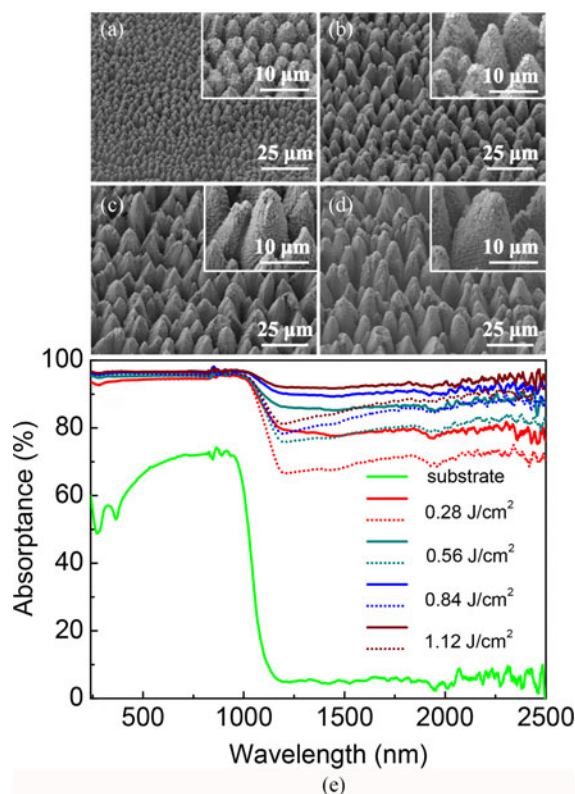
Fig. 1. (a)~(d) SEM images (tilt 45°) of phosphorus doped black silicon fabricated at different laser fluences. (a) 0.28, (b) 0.56, (c) 0.84, and (d) 1.12 J/cm^2. Scale bars are 25 μm for (a)~(d) and 10 μm for inserts. (e) Absorptance of crystalline silicon substrate and SPL1~SPL4 before annealing (solid lines) and after the annealing (dash dot lines).

The dashed dot curves in Fig. 1(e) show the absorptance after annealing for 30 min at 873 K in argon atmosphere. For all samples, annealing does not affect the absorption in the above-band-gap wavebands (or visible light region, $\lambda = 0.25 \sim 1.1 \, \mu$m) because the absorption enhancement in these wavebands is caused by the multiple reflections of light on the textured Si surface [15], [16], which is independent of thermal annealing. Unlike the absorptance in the visible light region, the absorptance in the infrared light region is reduced by different amounts, which vary from 5% to 15% after annealing. The remaining infrared absorptance is still very high (approximately 70% $\sim$ 88% for SPL1~SPL4@2 μm) compared to that of S-doped samples (approximately 5% $\sim$ 40%) [17], [18]. This relatively stable infrared absorption is caused by the weak P impurity diffusion process that occurs during annealing and can be attributed to the large separation coefficient and high solid solubility of P atoms in the Si substrate. Prior to the annealing, the high infrared absorption of P-doped B-Si is supposed to be induced by three mechanisms: Urbach states from α-Si or nanocrystal in the re-solidified surface layer [19], [20], deep-level absorption of structural defects induced by the fast melt cooling process [21], and free carrier absorption of the highly doped P impurities. In particular, all the infrared absorption can be enhanced by the geometric multiple reflection effect [29], [30]. After thermal annealing, the remaining absorption can be attributed to the free carrier absorption mechanism, which will be discussed in detail below.

Experiments have been conducted to obtain a further understanding of the dependence of the infrared absorptance on the annealing process. Here, ΔA is used to describe the reduction of absorptance caused by thermal treatment described by $\Delta A = A_b - A_a$. Here, A_b and A_a represent the absorptance of B-Si before and after annealing, respectively. Instead of using the absolute absorptance, we compared the ΔA values of different samples to eliminate the effect of sample-to-sample variations. P-doped B-Si samples fabricated using an fs laser at a laser fluence of 0.56 J/cm^2
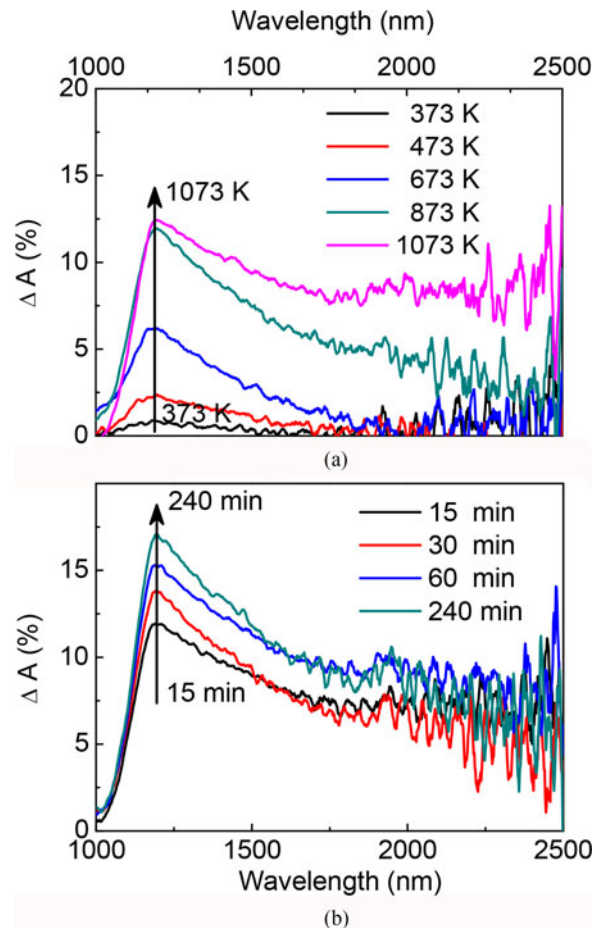
Fig. 2. (a) Absorptance decrement of phosphorus doped black silicon (SPL2) after the annealing for 30 min at different temperatures in argon atmosphere. (b) Absorptance decrement of phosphorus doped black silicon after the annealing at 873 K for different annealing time.

(the same as SPL2) are annealed in argon atmosphere for 30 min at different temperatures: 373, 473, 673, 873, and 1073 K. In Fig. 2(a), the $\triangle$A values of all five samples increase with the annealing temperature. In other words, a higher annealing temperature will lead to a larger absorptance reduction. At the near band edge wavelengths (from 1.1 to 1.7 μm), the absorptance decreases at all experimental temperatures (from 373 K to 1073 K). However, for longer wavelengths (from 1.7 to 2.5 μm), the absorptance remains unchanged until the annealing temperature rise to 873 K. Based on this phenomenon, it is assumed that different mechanisms contribute to the absorptance reduction at different temperatures. The reduction of absorptance in the wavelengths from 1.1 to 1.7 μm at low annealing temperatures may be due to the disappearance of structural defects related to the Urbach states that are known to introduce infrared-absorbing states near the band edge and are unstable with respect to the thermal treatment [18]–[20], [22]. When the temperature exceeds 873 K, the decrease in absorptance in the wavelength region from 1.1 μm to 2.5 μm is mainly caused by the reduction of deep level defects that are insensitive to low temperatures. According to Barhdadi's research [21], the deep level defects (e.g., the di-vacancy V-V, multi-vacancy center, vacancy-oxygen complex, clusters of vacancy, vacancy-impurity associations) can be generated when fluence is above the melting threshold and they are mostly generated from the fast quenching process during pulsed laser treatments. Fig. 2(b) shows the $\triangle$A values of P-doped B-Si samples after annealing at 873 K in argon atmosphere for different times ranging from 15 to 240 min. Examining the experimental curves indicates that the variations in absorptance increase
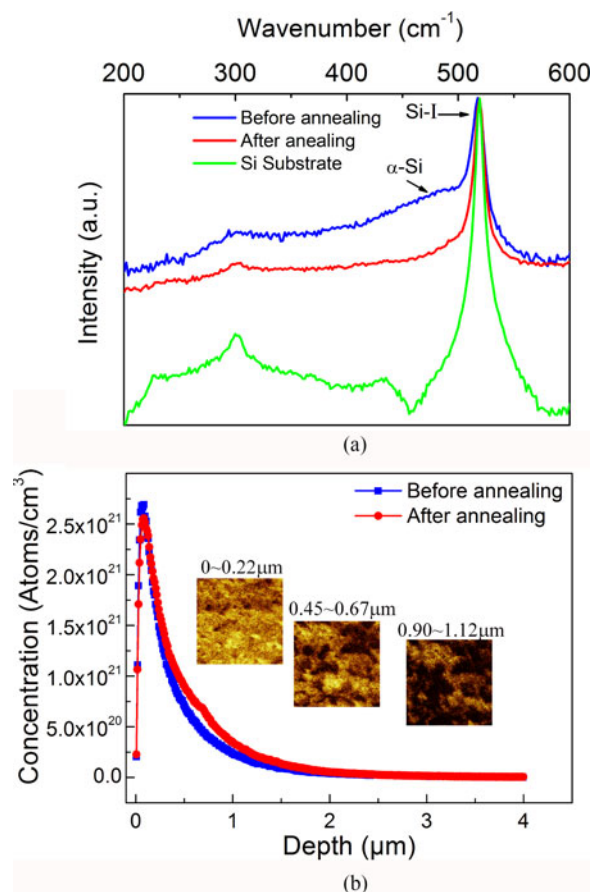
Fig. 3. (a) Raman spectra of SPL2, before annealing (blue line), annealing for 30 min at 873 K (red line), and spectra of crystalline silicon substrate (green line); (b) SIMS profiles of phosphorus doped silicon at a depth of 3 μm; inserts are the dopant distribution in a specific area for three different depths.

with annealing time because a longer annealing time can improve the lattice arrangement and then reduce the concentration of defects which lead to infrared absorption. However, increasing the annealing time or increasing the annealing temperature would not obviously reduce the infrared absorptance of P-doped B-Si. The $\triangle$A values for all P-doped samples are below 18%.

To investigate the crystal types in the re-solidified surface layer, the Raman spectrum of SPL2 was measured and is shown in Fig. 3(a). In addition to the crystalline Si (Si-I) peak at 520 cm^{-1}, two broad vibration peaks at 300 and 475 cm^{-1} are formed after the laser irradiation and correspond to the amorphous Si (α-Si) structure [23]. Unlike the S-doped B-Si, the Raman peaks assigned to the Si polymorphs, such as the R8 (Si-XII) and BC8 (Si-III) structures, are invisible [24]. Thus, the crystal quality of P-doped B-Si is better than that of the S-doped Si because substituted P atoms induce less lattice distortion in Si than do the substituted S atoms. After thermal annealing, the crystal quality improves slightly by removing one part of the metastable defects in α-Si.

Fig. 3(b) shows the concentration distribution of P impurities in the uppermost 4 μm of B-Si for the sample irradiated with 0.56 J/cm^2. The spectrum is obtained by sputtering the sample surface with Cs$^+$ while performing a second ion mass spectrometer scan. The image lateral resolution is less than 1 μm, and the impurity concentration is measured in a 20 $\times$ 20 μm^2 surface area (containing approximately 40 spikes) along the textured Si substrate. According to Fig. 3(b), the doping concentration of P is very high, reaching on the order of 10^{21} cm^{-3} in the surface layer and slowly decreases deeper into the sample. Unlike the S-doped B-Si, impurity diffusion after annealing for 30 min at 873 K is not obvious in the P-doped samples [17]. The P concentration
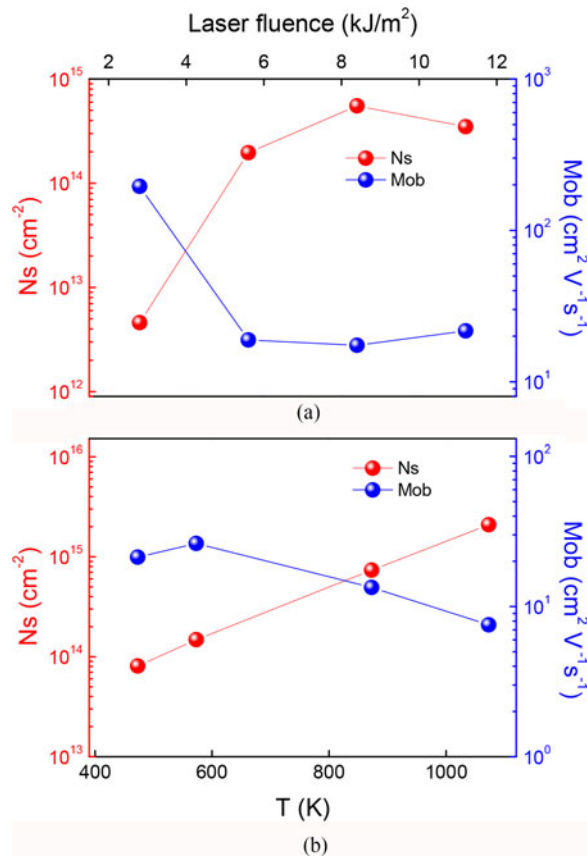
Fig. 4. (a) Hall-effect measurement for sheet carrier concentration and mobility of phosphorus doped silicon at different laser fluences; (b) Hall-effect measurement for sheet carrier concentration and mobility of phosphorus doped silicon at different annealing temperature.

remains nearly the same before and after annealing because although the doping concentration of P is very high, it is still of the same magnitude as the solubility limit of P, and the diffusion velocity of P in Si is low. The images in the inset of Fig. 3(b) show the P impurity distribution in the surface area for three specific depths (0~0.22, 0.44~0.67, and 0.90~1.12 μm) prior to annealing. These images indicate that the distribution of P atoms (golden points) is not uniform in the detecting region and that the impurity concentration decreases with depth.

The electronic nature of the P-doped layer of B-Si is probed via Hall Effect measurements. B-Si samples are cut into 10-mm squares, and 1-mm rounded-Indium (In) contacts are deposited at the four corners of these samples. The sheet electron density and carrier mobility of SPL1~SPL4 measured after the annealing are shown in Fig. 4(a). The given sheet carrier density of phosphorous doped layer of B-Si is directly measured by Hall Effect based on the van der Pauw technique [31]. Overall, the electron density of the P-doped samples increases with laser fluence because the laser irradiation increases the number of electrically active P impurities. Further, an increase in electron density can enhance the impurity scattering in the surface layer, which can lead to a drop in carrier mobility.

For a lower laser fluence of 0.28 J/cm^2, the melting and damaged regions ablated by fs laser irradiation are not uniform because the covering of phosphorous paper and the non-uniformity of laser fluence will lead to a lower total number of P dopants due to the local insufficient melting and ablation for a larger area Hall sample (10 $\times$ 10 mm^2). Therefore, the electronic density shows a lower measured value. However, for the higher laser fluence (0.56, 0.84, and 1.12 J/cm^2), the laser fluence that is received by the Si substrate will far outweigh the ablation threshold of the Si material.
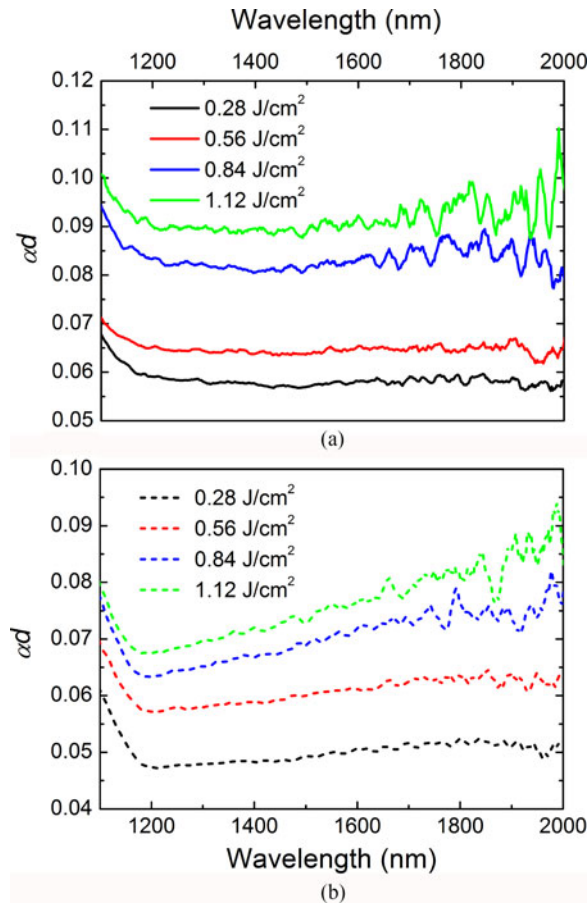
Fig. 5. (a) αd product of phosphorus doped black silicon SPL1~4. (b) αd product of SPL1~4 after the annealing at 873 K for 30 min in argon atmosphere.

Finally, the total number of phosphorus dopants for the Hall samples will increase with an increase in laser fluence. In addition, the change in the total number of dopants is not obvious and occurs more slowly because the phosphorous can be doped into Si nearly in all irradiated regions after the higher laser fluence irradiation. As a result, the dependence of sheet carrier density on laser fluence exhibits the tendency shown in Fig. 4(a), which is consistent with the change in the total number of phosphorus dopants in the Hall measurement samples. For comparison, we measured the sheet carrier densities of Si substrate and non-doped B-Si samples irradiated by fs laser without phosphorus paper covering, using the same laser fluence as for the data presented in Fig. 4(a). The sheet carrier density arising from the highly resistive Si substrate can be neglected because it is only 3.26×10^{10} cm^{-2}. Then, the sheet carrier density of all laser irradiated B-Si without covering of phosphorus is maintained on the order of 10^{12} cm^{-2} ($< 2.5 \times 10^{12}$ cm^{-2}), and the structural defects induced by fs laser ablation may contribute to this result. Except for the SPL1 sample that is affected seriously by the insufficient fs laser irradiation, this contrast shows that the sheet carrier density contributed by phosphorus doping is much higher than the contribution from the fs-laser-induced structural defects.

Fig. 4(b) shows the influence of the annealing temperature on the B-Si electrical properties. Four samples fabricated at the laser fluence of 0.56 J/cm^2 are annealed for 30 min at different temperatures of 473, 573, 873, and 1073 K. Annealing to a higher temperature increases the sheet electron density because the annealing causes a change in the local bonding/electronic environment of implanted atoms, thereby increasing the number of free carriers by decreasing the coordination number or annihilating defects [25].

To clarify the absorption contributions the αd product (α is absorption coefficient, d is absorption depth) for SPL1~SPL4 at infrared region are plotted in Fig. 5. The αd product is calculated from the measured R and T using $\alpha d = (1/m)\ln[(1-R)/T]$, where m is light tripping factor and all the absorption contributions can be enhanced by this factor and the maximum light tripping is assumed ($m = 49$) [30]. Here, even though the SIMS measurement data show that concentration of P dopant can reach to 10^{20} atoms/cm^3 at 1.5 μm depth, we convinced that the majority dopant and carriers are concentrated in re-solidified surface layer and the d of SPL2 can be assumed to 500 nm [32]. According to Fig. 5, the αd values increase with laser fluence both before and after annealing. For an identical sample, αd value decreases after thermal annealing; this is in accord with the absorption property. Before thermal annealing, the high infrared absorption in P-doped B-Si is a combination of free carrier absorption and Urbach state absorption. Structural defects absorption decreases with increasing wavelength (1.1~1.7 μm), whereas the free carrier absorption increases with increasing wavelength ($>$1.1 μm, $\alpha \propto \lambda^n$, n~2). Therefore, α values of P-doped B-Si remain nearly unchanged with increasing wavelength (see Fig. 5(a)). After thermal annealing, the infrared absorption induced by Urbach state and deep-level defects should be neglected due to the instability and the infrared absorption in Fig. 5(b) is contributed only from free carrier absorption. The measured α value is approximately 1224 cm^{-1}@2 μm for SPL2 in Fig. 5(b) of the annealed P-doped B-Si. According to Spitzer [26], [27], the maximum α value of Si would be anticipated to be 100 cm^{-1} @ 2 μm if the free carrier concentration is about 5×10^{18} cm^{-3} (calculated by N_s and d from SPL2). Obviously, there is about one order of magnitude discrepancy between measured and estimated α value and this is because the measured sheet carrier concentration is an average value of a non-uniform doping distribution, and this is further complicated by the non-uniform thickness and rough surface of the phosphorous doped layer [30].

4. Conclusion

Highly P-doped B-Si is obtained by femtosecond laser direct writing. The surface topography of the textured Si substrate fabricated at different laser fluence is characterized by SEM images. Both the dimension of spike microstructures and the absorptance of P-doped Si increase with laser fluence. Examining the UV-VIS-IR absorption spectra shows that the infrared absorptance of P-doped B-Si is nearly insensitive to thermal treatments and remains greater than 70% after annealing for 30 min at 873 K in argon atmosphere. The reduction in infrared absorptance is mainly caused by the disappearance of Urbach states in the re-solidified surface layer. Raman spectrum analyses show that P-doped B-Si exhibits a high crystallinity in the surface layer and that the crystal quality can be further improved by thermal annealing. Through SIMS measurement, the distribution of P impurity is quantitatively measured and is found to be as high as 10^{21} cm^{-3}. Thermal annealing has nearly no effect on the distribution of P impurities. The electronic properties, including sheet resistance and carrier motilities, are obtained by Hall Effect measurements. Both laser fluence and annealing duration affect the electronic properties of P-dopants in B-Si layer.

References

[1] T. H. Her, R. Finlay, J. C. Wu, and E. Mazur, "Femtosecond laser-induced formation of spikes on silicon," *Appl. Phys. A*, vol. 70, no. 4, pp. 383–385, 2000.
[2] C. Wu *et al.*, "Near-unity below-band-gap absorption by microstructured silicon," *Appl. Phys. Lett.*, vol. 78, no. 13, pp. 1850–1852, 2001.
[3] C. H. Crouch, J. E. Carey, M. Shen, E. Mazur, and F. Y. Génin, "Infrared absorption by sulfur-doped silicon formed by femtosecond laser irradiation," *Appl. Phys. A*, vol. 70, no. 7, pp. 1635–1641, 2004.
[4] M. Halbwax *et al.*, "Micro and nano-structuration of silicon by femtosecond laser: Application to silicon photovoltaic cells fabrication," *Thin Solid Films*, vol. 516, no. 20, pp. 6791–6795, 2008.
[5] Z. Huang, J. E. Carey, M. Liu, X. Guo, E. Mazur, and J. C. Campbell, "Microstructured silicon photodetector," *Appl. Phys. Lett.*, vol. 89, no. 3, 2006, Art. no. 033506.
[6] A. J. Said *et al.*, "Extended infrared photoresponse and gain in chalcogen-supersaturated silicon photodiodes," *Appl. Phys. Lett.*, vol. 99, no. 7, 2011, Art. no. 073503.

[7] R. G. Wilson, "Depth distributions of sulfur implanted into silicon as a function of ion energy, ion fluence, and anneal temperature," *J Appl. Phys.*, vol. 55, no. 10, pp. 3490–3494, 1984.

[8] M. T. Winkler, D. Recht, M. J. Sher, A. J. Said, E. Mazur, and M. J. Aziz, "Insulator-to-metal transition in sulfur-doped silicon," *Phys. Rev. Lett.*, vol. 106, no. 17, 2011, Art. no. 091106.

[9] Y. Peng *et al.*, "Annealing-insensitive "black silicon" with high infrared absorption," *J. Appl. Phys.* vol. 116, no. 7, 2014, Art. no. 073102.

[10] H. B. Normann, B. G. Svensson, and E. Monakhov, "Formation of shallow front emitters for solar cells by rapid thermal processing," *Phys. Status Solidi C*, vol. 9, no. 10/11, pp. 2138–2140, 2012.

[11] Y. F. Lao, A. G. Unil Perera, L. H. Li, S. P. Khanna, E. H. Linfield, and H. C. Liu, "Tunable hot-carrier photodetection beyond the bandgap spectral limit," *Nat. Photon.*, vol. 8, no. 5, pp. 412–418, 2014.

[12] J. Yan *et al.*, "Dual-gated bilayer graphene hot-electron bolometer," *Nat. Nanotech.*, vol. 7, no. 7, pp. 472–478, 2012.

[13] A. Martí *et al.*, "Production of photocurrent due to intermediate -to-conduction-band transitions: A demonstration of a key operating principle of the intermediate-band solar cell," *Phys. Rev. Lett.*, vol. 97, no. 24, 2006, Art. no. 247701.

[14] E. Antolín *et al.*, "Lifetime recovery in ultrahighly titanium-doped silicon for the implementation of an intermediate band material," *Appl. Phys. Lett.*, vol. 94, no. 4, 2009, Art. no. 042115.

[15] J. Yang *et al.*, "Design and fabrication of broadband ultralow reflectivity black Si surfaces by laser micro/nanoprocessing," *Light Sci. Appl.*, vol. 3, no. 7, 2014, Art. no. e185.

[16] R. Younkin, J. E. Carey, E. Mazur, J. A. Levinson, and C. M. Friend, "Infrared absorption by conical silicon microstructures made in a variety of background gases using femtosecond-laser pulses," *J. Appl. Phys.*, vol. 93, no. 5, pp. 2626–2629, 2003.

[17] B. R. Tull, M. T. Winkler, and E. Mazur, "The role of diffusion in broadband infrared absorption in chalcogen-doped silicon," *Appl. Phys. A*, vol. 96, no. 2, pp. 327–334, 2009.

[18] C. H. Crouch, J. E. Carey, J. M. Warrender, M. J. Aziz, E. Mazur, and F. Y. Génin, "Comparison of structure and properties of femtosecond and nanosecond laser-structured silicon," *Appl. Phys. Lett.*, vol. 84, no. 11, pp. 1850–1852, 2004.

[19] C. H. Li, J. H. Zhao, Q. D. Chen, J. Feng, W. T. Zheng, and H. B. Sun, "Infrared absorption of femtosecond laser textured silicon under vacuum," *IEEE Photon. Technol. Lett.*, vol. 27, no. 14, pp. 1481–1484, Jul. 2015.

[20] X. B. Li, X. Q. Liu, X. D. Han, and S. B. Zhang, "Role of electronic excitation in phase-change memory materials: A brief review," *Phys. Status Solidi B*, vol. 249, no. 10, pp. 1861–1866, 2012.

[21] A. Barhdadi, B. Hartiti, and J. C. Muller, "Active defects generated in silicon by laser doping process," *African Rev. Phys.*, vol. 6, pp. 229–238, 2011.

[22] W. B. Jackson, N. M. Johnson, and D. K. Biegelsen, "Density of gap states of silicon grain boundaries determined by optical absorption," *Appl. Phys. Lett.*, vol. 43, no. 2, pp. 195–197, 1983.

[23] V. Domnich and Y. Gogotsi, "Phase transformations in silicon under contact loading," *Rev. Adv. Mater. Sci.* vol. 3, no. 1, pp. 1–36, 2002.

[24] X. Dong *et al.*, "Strong mid-infrared absorption and high crystallinity of microstructured silicon formed by femtosecond laser irradiation in NF3 atmosphere," *Appl. Phys. Exp.*, vol. 6, no. 8, 2013, Art. no. 081301.

[25] J. E. Carey, "Femtosecond-laser microstructuring of silicon for novel optoelectronic devices," Ph.D. dissertation, Harvard Univ., Cambridge, MA, USA, 2004, pp. 80–81.

[26] W. Spitzer and H. Y. Fan, "Infrared absorption in n-type silicon," *Phys. Rev.*, vol. 108, no. 2, pp. 268–271, 1957.

[27] T. G. Kim, J. M. Warrender, and M. J. Aziz, "Strong sub-band-gap infrared absorption in silicon supersaturated with sulfur," *Appl. Phys. Lett.*, vol. 78, no. 24, 2001, Art. no. 241902.

[28] R. Younkin, "Surface studies and microstructure fabrication using femtosecond laser pulses," Ph.D. dissertation, Harvard Univ., Cambridge, MA, USA, 2001.

[29] Y. F. Huang *et al.*, "Improved broadband and quasi-omnidirectional anti-reflection properties with biomimetic silicon nanostructures," *Nat. Nanotech.*, vol. 2, no. 12, pp. 770–774, 2007.

[30] M. J. Sher, Y. T. Lin, M. T. Winkler, E. Mazur, C. Pruner, and A. Asenbaum, "Mid-infrared absorptance of silicon hyperdoped with chalcogen via fs-laser irradiation," *J. Appl. Phys.*, vol. 113, no. 6, 2013, Art. no. 063520.

[31] L. J. van der Pauw, "A method of measuring the specific resistivity and hall effect on discs of arbitrary shapes," *Philips Res. Repts.*, vol. 13, no. 1, pp. 1–9, 1958.

[32] M. J. Sher, M. T. Winkler, and E. Mazur, "Pulsed-laser hyperdoping and surface texturing for photovoltaics," *MRS Bull.*, vol. 36, no. 6, pp. 439–445, 2011.